AN OPTIMIZATION OF PERFORATION DESIGN ON A PIEZOELECTRIC-BASED SMART STENT FOR BLOOD PRESSURE MONITORING AND LOW-FREQUENCY VIBRATIONAL ENERGY HARVESTING

Jun Ying Tan[1], Sayemul Islam[2], Yuankai Li[3], Albert Kim[2], and Jungkwun 'JK' Kim[1]
[1]Department of Electrical Engineering, University of North Texas, Denton, TX 76207, USA.
[2]Department of Medical Engineering, the University of South Florida, Tampa, FL 33620, USA.
[3]Department of Electrical and Computer Engineering, Kansas State University, Manhattan, KS 66506, USA.

2023 IEEE 36th International Conference on Micro Electro Mechanical Systems (MEMS) | 978-1-6654-9308-6/23/$31.00 ©2023 IEEE | DOI: 10.1109/MEMS49605.2023.10052623

ABSTRACT

This paper presents the perforated design of a piezoelectric tube that will be employed as a self-powered Smart Stent for real-time blood pressure monitoring. The proposed Smart Stent was made of polyvinylidene fluoride (PVDF), which can harvest energy from pulse-motion low-frequency vibration such as blood flow. This study focuses on a unique pattern of the perforation added to the Smart Stent. We observed that the perforation design of Smart Stent varies its sensitivity to pressure change and produces different energy harvesting performances. The eight different perforations design of the Smart Stent were fabricated, examined, and reported their performances.

KEYWORDS

Smart Stent, piezoelectric, pressure sensor, low-frequency energy harvester, implantable medical device.

INTRODUCTION

Abdominal aortic aneurysm (AAA) accounts for approximately 60% of mortality once it ruptures [1]. A common preventative treatment, known as endovascular aneurysmal repair (EVAR), has been a popular intervention by which placing a fabric-covered stent graft at the abnormal site to redirect the blood flow away from the aortic wall [2]. The practice of EVAR has a lower 30-day postoperative mortality rate of 3.5% compared to 7.1% for conventional open surgical repair [3]. It also reduced time under general anesthesia [4], length of stay in the hospital and intensive care unit (ICU) [5], and likelihood of intraoperative blood transfusions [6], [7]. Despite the advantages, a fatal mechanical failure of the stent, known as endoleak, has remained unsolved [8], [9]. Hence, a post-EVAR surveillance is recommended. Radiography, ultrasonography, computed tomography (CT), nuclear imaging, magnetic resonance angiography (MRA), and conventional angiography are the current post-EVAR surveillance techniques [8]. However, these techniques are expensive and require trained personnel, while some might require an invasive procedure, long scanning time and could cause radiation exposure [8].

Previously, we demonstrated a Smart Stent system that can measure the blood flow information wirelessly through an ultrasonic excitation [10]. In this work, we further explore the Smart Stent as a pressure sensor and energy harvester based on a similar architecture. The Smart Stent simultaneously harvests ambient vibrational energy (i.e., blood flow) while monitoring the blood pressure at the implanted site in real time. The harvested energy can be used to power the transmission circuit and other implanted devices to eliminate the necessity for an external source.

To achieve that, we incorporate a custom-perforated, piezoelectric-based Smart Stent that can be deployed onto the stent graft, as shown in Fig. 1. The function of the perforation has been discussed in the previous study [10]. In short, it induced a negative Poisson's ratio (NPR) of the Smart Stent, which allows it to expand transversely under axial strain. However, the previous design was characterized to enhance ultrasonic powering efficiency, while the proposed Smart Stent aimed to harvest low-frequency vibrational energy from blood flow (1 to 1.67 Hz or 60 to 100 beats per min). Therefore, it is necessary to optimize the perforation design.

In this paper, the perforation design was characterized based on the size, orientation, and shape of the perforation. Eight types of perforation designs were demonstrated including seven perforated samples and one unperforated sample as a control. All Smart Stents had the same length and diameter of 70 and 14.5 mm, respectively. The Smart Stents were examined in a closed-loop circulation system and a complete set of experimental results were reported. The optimum design is recommended based on the sensitivity to pressure change and the magnitude of generated voltage.

MATERIALS AND FABRICATION

Poly(vinylidene fluoride) (PVDF) powder and N, N-Dimethylformamide (DMF) 99% were purchased from Alfa Aesar Chemicals. Polydimethylsiloxane (PDMS) elastomer was purchased from Dow Corning Corporation.

The fabrication process of the Smart Stent is depicted in Fig. 2. The PVDF film casting was based on Cardoso et al.'s work [11]. In brief, 15 wt. % of PVDF solution was prepared by dissolving the PVDF powder in DMF solution, and continuously mixing with a magnetic stirrer for 15 min at 30 °C. The substrate for film casting was a 2" × 3" glass slide, that had been cleaned with organic solvents (acetone, methanol, and isopropanol), dried with nitrogen, and

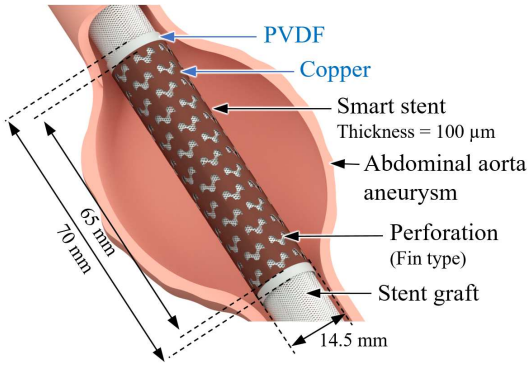

Figure 1: Conceptual drawing of a Smart Stent mounted on a stent graft in an abdominal aorta aneurysm.

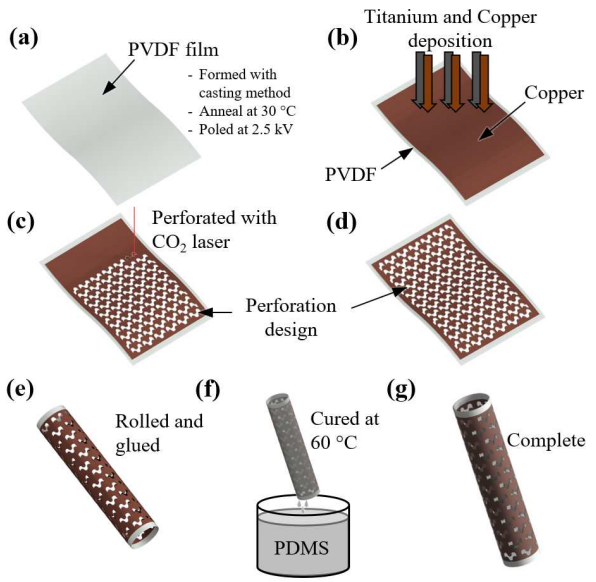

Figure 2: Fabrication process of the Smart Stent. (a) PVDF film. (b) Metallization. (c) Laser machining. (d) Perforated film. (e) Rolled to form tube. (f) PDMS passivation. (g) Smart Stent complete.

treated with oxygen plasma to remove all potential contaminants. 3 g of the PVDF solution was cast onto the glass slide and allowed to spread until uniform thickness was achieved. The sample was annealed for at least 24 h at 30 °C and 30% humidity. Once dried, the PVDF film was delaminated from the glass slide by immersing the sample in deionized (DI) water for 5 min due to hydrophobicity. For poling, the film was sandwiched between two electrodes and applied voltage of 2.5 kV for 1 h at 80 °C. A 100-µm PVDF film was obtained via this process as shown in Fig. 2(a). The film was metalized on both sides with titanium (100 nm) and copper (300 nm) using a DC sputter as depicted in Fig. 2(b). For perforation, the metalized film was laser-machined with a CO_2 laser with 22.5 W at cutting speed of 200 mm/s as illustrated in Fig. 2(c-d). The perforated film was rolled into a tube and glued together using DMF solution as demonstrated in Fig. 2(e). The sample was dip-coated into a PDMS solution for passivation, cured at 60 °C for 3 hours as shown in Fig. 2(f), and the completed Smart Stent is shown in Fig. 2(g).

PERFORATION DESIGNS AND SETUP

The perforation designs of the Smart Stent were characterized based on the pore size (defined as "big" or "small"), orientation (i.e., normal or parallel), and shape (i.e., fin or wave). The combination of these features results in eight different perforation designs, as listed in Table 1. The acronym of each design is derived from its corresponding features, for instance, BNF is short for a sample with big-sized (B), normally-oriented (N), and fin-shaped (F) perforation. Note that the BNF sample was adopted from our previous work [10]. In addition, an unperforated sample was included as a control, abbreviated as "plain."

A closed-loop circulation system was prepared to examine the Smart Stents, which consists of a DI water reservoir, two peristaltic pumps, a 3D printed abdominal aorta model, a pressure gauge, a roller clamp, and a Smart Stent as shown in Fig. 3. The abdominal aorta model was 3D printed with a flexible resin (Elastic 50A, Formlabs Inc.). A pressure gauge was installed as close to the model as possible to monitor the water pressure prior entering the model. A constant flow of DI water was pumped by peristaltic pump 1 to maintain a steady 80 mmHg pressurized environment inside the model. In the meantime, the peristaltic pump 2 was programmed to intermittently pump pulses of water with 40 mmHg, which result in a cumulative pressure of 120 mmHg inside the model. The pressure can be adjusted based on the water volume that was pumped into the model by pump 1 and 2, where pump 1 defines the diastolic pressure and pump 2 defines the systolic pressure, typically, 80/120 mmHg was used. The roller clamp at the end of the model was used to fine tune the pressure. In order to monitor the Smart Stents after being implanted into the system, wires were connected on each side of the Smart Stent to enable measuring the induced voltage via an oscilloscope (Analog Discovery 2, Digilent) and a computer. A ground bar (GND) was introduced in the system to eliminate the 60 Hz noise. Due to the limitation of the peristaltic pumps, the fastest pulse rate that can be generated by the described system was 30 pulses per minute (0.5 Hz), which is less than the typical human heart rate of 60 to 100 beats per minute (1 to 1.67 Hz). Nonetheless, this limitation does not impair the experiment in determining the optimal

Table 1. Parameters of the perforation designs

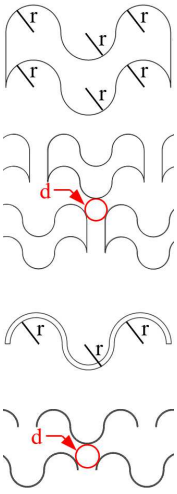

Size	*Orientation*	*Shape*	*Acronym*	*Radius (r) [mm]*	*Gap Size (d) [mm]*	*No. of perforation*	*Area loss (%)*
N/A	N/A	N/A	Plain	N/A	N/A	0	0
Big	Normal	Fin	BNF	1.8	2.50	24	29.62
Small	Normal	Fin	SNF	0.9	1.25	96	29.62
Small	Parallel	Fin	SPF	0.9	1.25	100	30.86
Big	Normal	Wave	BNW	1.8	2.70	39	3.57
Big	Parallel	Wave	BPW	1.8	2.70	45	4.12
Small	Normal	Wave	SNW	0.9	1.35	182	8.33
Small	Parallel	Wave	SPW	0.9	1.35	180	8.24

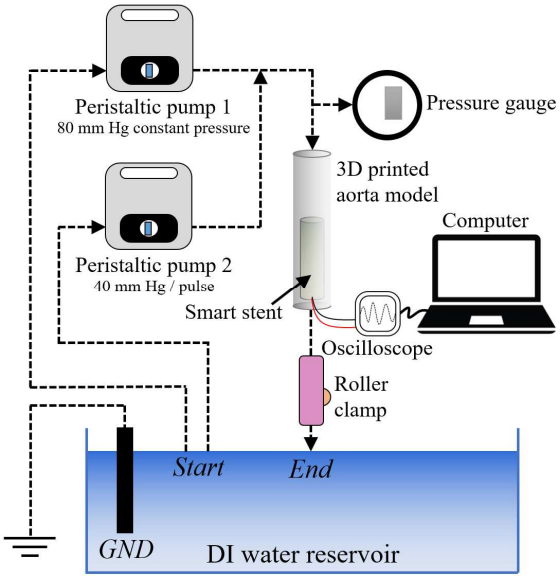

Figure 3: Experimental setup of a closed-loop circulation system for testing the Smart Stents.

perforation design on the Smart Stent as the pulse rate does not affect the generated voltage.

RESULTS AND DISCUSSION

Figure 4(a-h) present the fabrication results of eight types of Smart Stents, including plain (control), BNF, SNF, SPF, BNW, BPW, SNW, and SPW. All Smart Stents were evaluated in the described system to determine their sensitivity to pressure change and voltage generation. All samples were tested at least three times and the average values were reported with corresponding standard deviation. All samples were wired and implanted into the system, and the results were shown in Fig. 5.

Figure 5(a) shows a 30-second continuous measurement of the voltage generated by the SNF sample in three different scenarios. The first scenario was represented by the black line, showing that the Smart Stent generated a steady voltage of 110 mV under 80 mmHg while the pump 1 was turned on and pump 2 remained off. The ripples were induced by the vibration caused by pump 1. The magnitude of the ripples was measured of approximately 1 mV, which is less than 1% of the measured voltage, and thus, negligible. This result demonstrates the stability of the system and the reliability of the Smart Stents. The second scenario was presented in blue line, with pump 1 constantly on, and pump 2 on intermittently, imitating the typical blood pressure variation of 80 to 120 mmHg every pulse. In this case, the voltage increased from 110 to 180 mV at each pulse, then decreased to 110 mV as the pulse pressure released. A maximum of 2.5% variation of the peak values was measured throughout the 30-second measurement, indicating the precision of the device. The third scenario, depicted in red line, had pump 1 constantly on, while pump 2 was on intermittently with lower pulse pressure of 10 mmHg, resulting in a cumulative pressure of 90 mmHg at each pulse. The described scenario imitated the situation when an endoleak or malfunction occurred in the system, which resulted in a drop in pulse pressure. The peak voltage was reduced to roughly 140 mV in response to the decreased pulse pressure, confirming its applicability as an early warning indication for endoleak.

Figure 5(b) shows the comparison of the Smart Stent's sensitivity with different perforation designs in response to pressure change. It should be noted that the legends were arranged in descending order in terms of the measured peak-to-peak voltage to better analyze the data. Among the seven perforated samples, all small-sized perforated samples (SPF, SPW, SNW, SNF) have demonstrated significant improvement in sensitivity to pressure change in comparison to the plain sample, whereas the big-sized perforated samples (BNW, BPW, BNF) appeared to perform worse. This result suggests that by introducing small-sized perforation on the Smart Stent, the sensitivity to pressure change can be improved up to 40%.

To evaluate the feasibility of the Smart Stents as low-frequency energy harvester, the average voltages generated by the Smart Stents were analyzed, and the result is shown in Fig. 5(c). Similarly, the legends were arranged in descending order in terms of the average voltage. Based on the results, SNW and SNF outperformed the plain sample in voltage generation, whereas the other perforated samples were inferior to the plain sample. The orientation of the perforation was critical in determining the magnitude of the generated voltage. Among the small-sized perforated samples, the normally perforated samples (SNW and SNF) have a positive impact on voltage generation, whereas the parallelly perforated samples (SPW and SPF) have a negative impact. However, of the two samples (SNW and SNF) that have positive impact, the SNW sample has received a 30% increase in voltage generation over the plain sample, while the SNF sample only received roughly 5% increment. This is due to the perforation shape, where the SNF sample has lost about 30% of its piezoelectric material, while the SNW sample only lost about 8%. In addition, the footprint's size of the wave pattern is smaller than the fin pattern, which 182 wave-patterns can fit onto the SNW sample while only 96 fin-patterns on the SNF sample. Similar results were observed in other comparison such as BNW and BNF, and SPW and SPF samples, where wave-shaped perforated samples yielded higher voltage than the fin-shaped perforated samples. In low frequency voltage generation, the wave-shaped perforation has shown superiority over fin-shaped perforation.

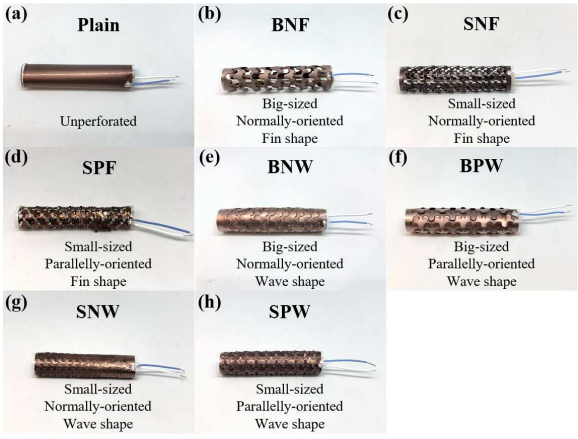

Figure 4: Fabrication results of the Smart Stents. (a) Plain. (b) BNF. (c) SNF. (d) SPF. (e) BNW. (f) BPW. (g) SNW. (h) SPW.

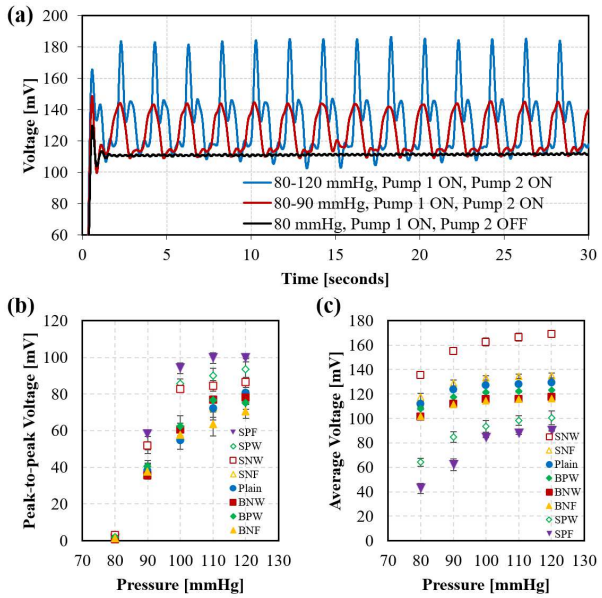

Figure 5: Experimental results of the Smart Stents. (a) 30-s continuous measurement of the SNF sample at 80, 90, and 120 mmHg cumulative pressure. (b) Sensitivity and (c) voltage generation of the Smart Stents.

CONCLUSIONS

With the perforation design as proposed, Smart Stent with 29.62% loss in piezoelectric material, such as the SNF sample, was able to generate higher voltage than the plain sample with better sensitivity to pressure change. The size of the perforation showed great importance in determining the device's sensitivity to pressure change, with small-sized perforation favored over big-sized perforation. The orientation of the perforation also highly affects the device's sensitivity and generated voltage. Parallelly-perforated samples are desirable for increasing the device sensitivity, whilst normally-perforated samples are desirable for higher voltage generation. Lastly, the shape of the perforation plays crucial role in the perforation design of the Smart Stents. Although there is no significant effect on the device sensitivity, it has considerable effect on the magnitude of the generated voltage, where wave-shaped perforation offers superior performance over fin-shaped perforation. In consideration of all the aforementioned parameters, the SNW sample has the optimum perforation design on the Smart Stent as pressure sensor and low-frequency energy harvester. Although SPF and SPW samples have offered excellent sensitivity to pressure change, their poor voltage generation hinders their practicality as Smart Stent. Considering the Smart Stent will be required to sustain other integrated circuits, especially a transmission circuit for wireless monitoring, a full-wave bridge rectifier integrated chip (IC) is needed to be integrated onto the device. While the IC typically requires at least 100 mV of forward voltage drop to operate, neither the SPF nor the SPW samples generate 100 mV or more under ideal conditions, rendering them ineffective as energy harvesters. In contrast, the SNW sample generated the highest voltage at various pressures while being moderately sensitive to pressure change, making it the optimum perforation design on the Smart Stent for pressure sensing and low-frequency, passive energy harvesting.

ACKNOWLEDGEMENTS

The research was supported by National Science Foundation (NSF) CNS 2039014, ECCS 2054567, ECCS 2029086, and ECCS 2029077.

REFERENCES

[1] Z. Yuan, Y. Lu, J. Wei, J. Wu, J. Yang, and Z. Cai, "Abdominal Aortic Aneurysm: Roles of Inflammatory Cells," *Frontiers in Immunology*, vol. 11, 2021.

[2] A. England and R. Mc Williams, "Endovascular Aortic Aneurysm Repair (EVAR)," *Ulster Med J*, vol. 82, no. 1, pp. 3–10, Jan. 2013.

[3] R. Greenhalgh, "Comparison of endovascular aneurysm repair with open repair in patients with abdominal aortic aneurysm," *The Lancet*, vol. 364, no. 9437, pp. 843–848, Sep. 2004.

[4] D. A. Bettex, M. Lachat, T. Pfammatter, D. Schmidlin, M. I. Turina, and E. R. Schmid, "To Compare General, Epidural and Local Anaesthesia for Endovascular Aneurysm Repair (EVAR)".

[5] G. Soulez *et al.*, "Pain and Quality of Life Assessment after Endovascular Versus Open Repair of Abdominal Aortic Aneurysms in Patients at Low Risk," *Journal of Vascular and Interventional Radiology*, vol. 16, no. 8, pp. 1093–1100, Aug. 2005.

[6] M. V. Raval and M. K. Eskandari, "Outcomes of elective abdominal aortic aneurysm repair among the elderly: Endovascular versus open repair," *Surgery*, vol. 151, no. 2, pp. 245–260, Feb. 2012.

[7] D. L. Davenport, S. D. O'Keeffe, D. J. Minion, E. E. Sorial, E. D. Endean, and E. S. Xenos, "Thirty-day NSQIP database outcomes of open versus endoluminal repair of ruptured abdominal aortic aneurysms," *Journal of Vascular Surgery*, vol. 51, no. 2, pp. 305-309.e1, Feb. 2010.

[8] D. Daye and T. G. Walker, "Complications of endovascular aneurysm repair of the thoracic and abdominal aorta: evaluation and management," *Cardiovasc Diagn Ther*, vol. 8, no. Suppl 1, pp. S138–S156, Apr. 2018.

[9] H. O. Kim, N. Y. Yim, J. K. Kim, Y. J. Kang, and B. C. Lee, "Endovascular Aneurysm Repair for Abdominal Aortic Aneurysm: A Comprehensive Review," *Korean J Radiol*, vol. 20, no. 8, p. 1247, 2019.

[10] S. Islam, X. Song, E. T. Choi, J. Kim, H. Liu, and A. Kim, "In Vitro Study on Smart Stent for Autonomous Post-Endovascular Aneurysm Repair Surveillance," *IEEE Access*, vol. 8, pp. 96340–96346, 2020.

[11] V. F. Cardoso, G. Minas, C. M. Costa, C. J. Tavares, and S. Lanceros-Mendez, "Micro and nanofilms of poly(vinylidene fluoride) with controlled thickness, morphology and electroactive crystalline phase for sensor and actuator applications," *Smart Materials and Structures*, vol. 20, no. 8, p. 087002, Jul. 2011.

CONTACT

*Jungkwun 'JK' Kim, tel: +1-940-369-7027; jungkwun.kim@unt.edu